

Single-Walled Carbon Nanotube Scaffolds for Dye-Sensitized Solar Cells

Patrick Brown, Kensuke Takechi, and Prashant V. Kamat*

Radiation Laboratory, Departments of Chemistry & Biochemistry and Chemical & Biomolecular Engineering, University of Notre Dame, Notre Dame, Indiana 46556-0579

Received: November 9, 2007; In Final Form: December 21, 2007

The influence of single-walled carbon nanotube (SWCNT) architectures for facilitating charge transport in mesoscopic semiconductor films has been probed using a TiO₂/Ru(II) trisbipyridyl complex system. Both transient absorption and emission measurements indicate that the SWCNT network in the film has no noticeable influence on the charge injection process from the excited Ru(II) trisbipyridyl complex into TiO₂ particles. However, it plays an important role in improving the charge separation, as the rate of back electron transfer between the oxidized sensitizer (Ru(III)) and the injected electrons becomes slower in the presence of the SWCNT scaffold. The beneficial aspect of charge collection by SWCNT has been further explored by carrying out photoelectrochemical measurements. The dye-sensitized solar cells constructed using this SWCNT scaffold show an improvement in the photocurrent generation. However, this improvement in photocurrent generation is neutralized by a lower photovoltage as the apparent Fermi level of the TiO₂ and SWCNT composite becomes more positive than that of pristine TiO₂.

Introduction

Nanostructured semiconductor films have been found useful for designing solar cells.^{1–3} The dye-sensitized solar cell (DSSC), which uses mesoscopic TiO₂ films modified with sensitizing dyes, has drawn significant attention as it can harvest visible light quite efficiently. Although power conversion efficiencies of the order of 10% have been attained with DSSC, further improvements in the performance of these solar cells are necessary.^{4,5} A major bottleneck, electron transport across the semiconductor particle network, often limits the performance of these solar cells. The grain boundaries encountered during the transit can result in electron recombination before they are efficiently collected at the electrode surface.^{6–8}

Semiconductor nanotube or nanowire assemblies, when assembled on the electrode surface and then modified with dye molecules, offer the possibility to improve the charge collection and transport of charge carriers. Such one-dimensional nanostructures have recently been shown to direct the flow of photogenerated charge carriers in DSSCs^{9–15} and quantum dot solar cells.^{16,17} Another approach involves the use of a SWCNT network on a conducting electrode surface to promote charge transport in mesoscopic TiO₂ films. The electrons injected from the excited dye into TiO₂ nanoparticles are then transferred through a SWCNT scaffold to generate photocurrent. The semiconducting property of SWCNT has been successfully exploited to improve the performance of organic photovoltaic cells¹⁸ and fuel cells.^{19,20} These two approaches that illustrate the role of 1-D architectures in facilitating electron transport in light harvesting nanoassemblies are shown in Scheme 1.

An effort was recently made to organize semiconductor (CdS, CdSe, CdTe) quantum dots on SWCNTs.^{21–28} The electron-accepting ability of semiconducting SWCNTs thus offers an opportunity to facilitate electron transport and increase the photoconversion efficiency of nanostructured semiconductor-based solar cells.^{29,30} By employment of a SWCNT network as

a conducting scaffold, we were able to achieve 2-fold enhancement in the photocurrent generation of TiO₂ particulate films.^{31,32} The organization of photoactive donor acceptor assemblies (e.g., porphyrin and C₆₀) on the electrode surface has already been shown to offer significant enhancement in the photoconversion efficiency of solar cells.^{33–36} The obvious questions that arises is: *Can one extend this strategy (Scheme 1) to improve the performance of DSSCs?* How does the conducting SWCNT scaffold influence the forward and back electron-transfer processes?

To address these questions, we have created SWCNT networks on conducting glass electrodes. TiO₂ nanoparticles are dispersed on this conducting scaffold of SWCNT and then modified with the Ru(bpy)₂(dcbpy)²⁺ complex. Spectroscopic and photoelectrochemical measurements that highlight the influence of SWCNT in modulating the charge separation and photocurrent generation are described.

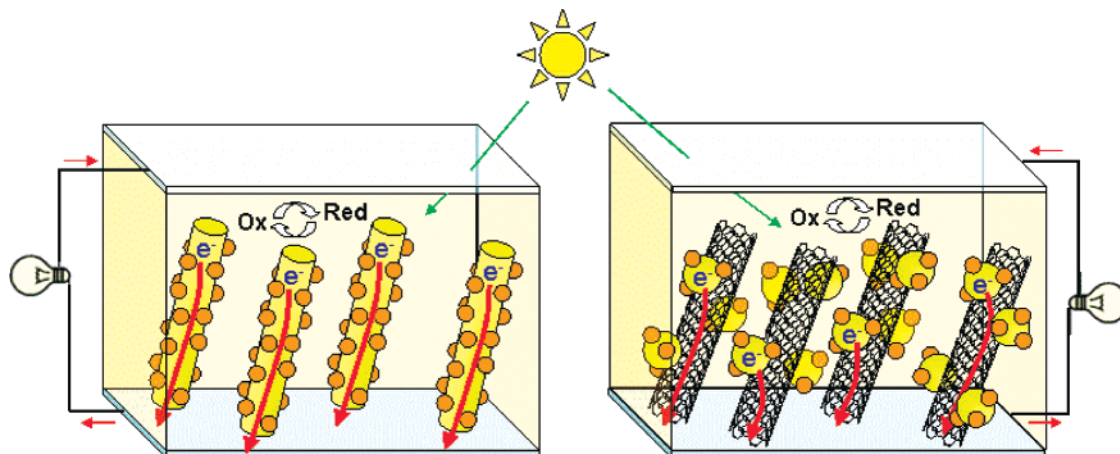
Experimental Section

Electrophoretic Deposition of SWCNT Films. Purified SWCNTs purchased from SES Research were used as received. The SWCNTs were solubilized in an organic solvent by sonication in tetrahydrofuran (THF) containing ~0.2 M tetraoctylammonium bromide (TOAB) and assembled as a thin film on optically transparent electrode (OTE) using the electrophoretic deposition technique.³⁷ A known amount of TOAB-solubilized SWCNT suspension in THF (0.01 mg/mL unless otherwise noted) was transferred to a 1-cm cuvette in which the OTE and a counter electrode (another OTE) were kept at a distance of 4 mm. A direct current voltage (50 V/cm) was applied between the electrodes using a Fluke 415 power supply. The deposition of the film can be monitored visibly as the SWCNT are driven to the electrode and the solution becomes colorless. These electrodes coated with SWCNT film are referred to as OTE/SWCNT.

TiO₂ Electrodes. TiO₂ colloids were formed by the hydrolysis of titanium(IV) isopropoxide in an aqueous mixture of acetic

* To whom correspondence should be addressed. E-mail: pkamat@nd.edu.

SCHEME 1: Directing the Flow of Photogenerated Electrons Across Nanostructured Semiconductor Films: (A) Nanotube/Nanowires Modified with Light-Absorbing Dye Molecules and (B) Nanotubes as Support Architecture for Anchoring Dye Modified Semiconductor Nanoparticles



acid and nitric acid. After refluxing for 2 h, the mixture was heated for 12 h at 500 K in an autoclave and washed with 5% nitric acid. Triton-X100 was added as a surfactant, and the mixture was ground with a mortar and pestle to break up any large particles, after which 5% nitric acid was added to bring the TiO₂ concentration to 20% by weight. The resulting paste was spread on OTE and OTE/SWCNT via the doctor blade technique and annealed in air at 473 K for 1 h. The electrodes were dyed overnight (~12 h) in a ~1 mM solution of Ru(bpy)₂-(dcbpy)²⁺ in ethanol. These electrodes are referred to as OTE/TiO₂/Ru(II) and OTE/SWCNT/TiO₂/Ru(II).

Optical Measurements. Absorption spectra were recorded using a Varian CARY50 Bio UV–Visible spectrophotometer. Emission spectra were recorded using an SLM 8100 photon-counting spectrofluorimeter. Emission lifetimes were measured using a Horiba Jobin Yvon single photon counting system, and the fluorescence lifetime decay data was analyzed using the IBH Datastation.

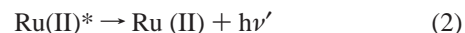
Transient Absorption Spectroscopy. Nanosecond transient absorption measurements were carried out with a 355-nm laser pulse from a Quanta Ray Nd:YAG laser system. OTE were loaded into a high-vacuum cell fitted with a 1-cm quartz cuvette. The films were arranged at a 45° angle, with excitation at the front face and emission monitored from the back face. The samples were evacuated for 2 h prior to the measurement. Femtosecond transient absorption measurements were conducted with a Clark-MXR 2010 laser system and an optical detection system provided by Ultrafast Systems (Helios) as described previously.²¹ All measurements were conducted at room temperature.

Photoelectrochemical Measurements. A thin-layer electrochemical cell with a 5-mm path length and two side arms for inserting reference (saturated Ag/AgCl) and counter (Pt gauze) electrodes was employed. All photoelectrochemical measurements were carried out in acetonitrile containing 0.5 M LiI and 0.05 M I₂ as electrolyte, with illumination from the back face of the OTE. A 450-W Xe arc lamp (Varian) with a copper sulfate filter (>300 nm) and UV cutoff filter (>380 nm) was employed as an excitation source. The intensity of the incident light near the electrode surface corresponded to 100 mW/cm². Incident photon to charge carrier efficiency (IPCE) measurements were carried out using a Bausch & Lomb high-intensity grating monochromator and no UV cutoff filter. Photocurrents at different applied potentials were measured using a Princeton Applied Research model PARSTAT 2263 potentiostat.

Results and Discussion

Morphology of Electrodes Composed of SWCNT and TiO₂. The scanning electron micrographs (SEM images) of conducting glass electrodes (OTE) modified with SWCNT and SWCNT–TiO₂ films are shown in Figure 1. These images provide a close look at the electrode morphology. The side view and the top view (A) of the OTE/SWCNT in Figure 1 show the network of carbon nanotubes that will serve as a support structure to anchor semiconductor nanoparticles. TiO₂ particles were then deposited on the SWCNT film. These TiO₂ nanoparticles attached to the SWCNT network provide a complete coverage and maintain a mesoscopic morphology. The SWCNT scaffold buried within the particulate film is thus expected to communicate with the TiO₂ particle network. Both OTE/TiO₂ and OTE/SWCNT/TiO₂ films were immersed in an ethanol solution of Ru(II)(bpy)₂(dcbpy) (henceforth referred to as Ru(II)) for several hours to facilitate the binding of the dye to the TiO₂ surface. The absorption spectra recorded in Figure 1C show the absorption band, with a maximum around 470 nm. The increased absorbance in trace e corresponds to a roughly 2.3% increase in absorbed light and can be attributed to the presence of the SWCNT film, which absorbs <5% of the incident light. Electrodes prepared by this method were employed in spectroscopic and photoelectrochemical measurements.

Charge Injection Process. Films of TiO₂ particles respond only to UV light as they undergo charge separation upon band gap excitation ($E_g > 3.2$ eV). When modified with a sensitizer such as Ru(II)(bpy)₂(dcbpy), the TiO₂ particles directly interact with the excited-state of the sensitizer via a charge-transfer mechanism (reactions 1–4)



The excited-state of the sensitizer (Ru(II)*) serves as an excellent probe to follow the forward electron-transfer processes in TiO₂–Ru(II) systems. Several research groups have extensively elucidated the charge transfer interaction between sensitizing dyes and TiO₂ particles.^{7,38–48} In the following discussion we will present spectroscopic and photoelectrochemical results and

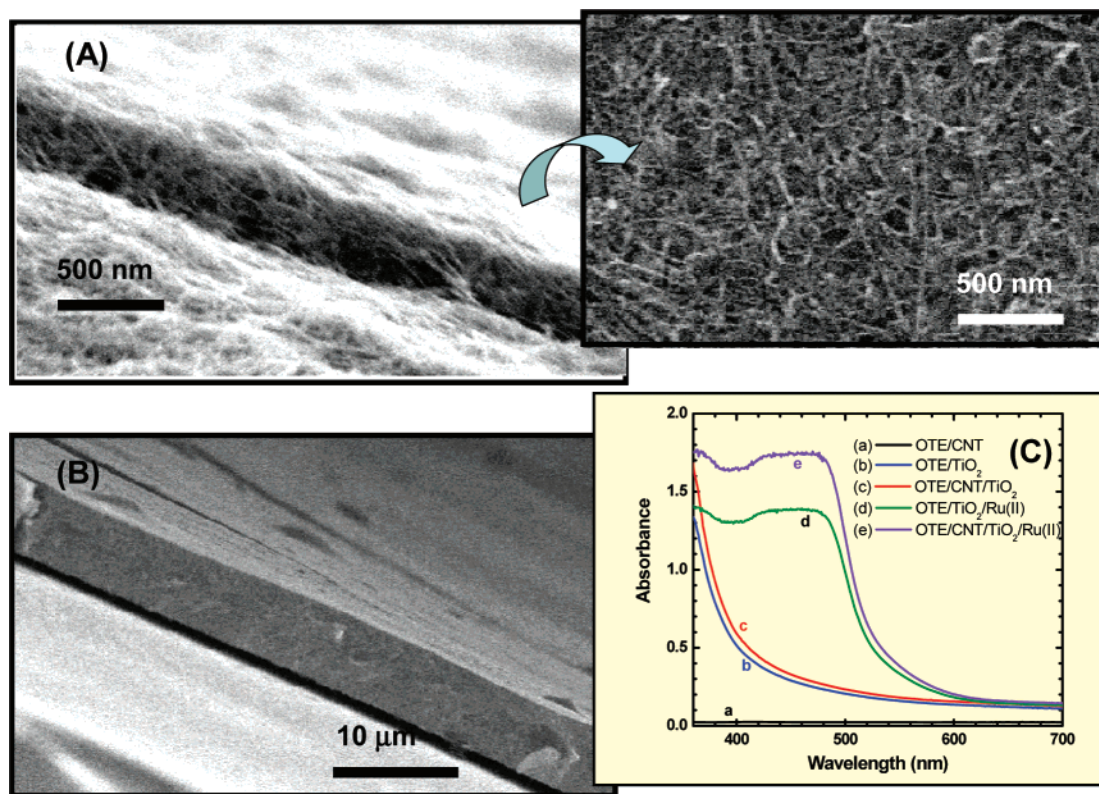


Figure 1. SEM of optically transparent electrode (OTE) (A) modification with SWCNT (sideview of a cracked film and top surface); (B) after deposition of TiO₂ particles onto SWCNT film; (C) absorption spectra of TiO₂ and SWCNT/TiO₂ films before and after modification with Ru(II) complex using OTE as reference. The difference in absorption between spectra d and e is mainly due to the SWCNT absorption (spectrum a).

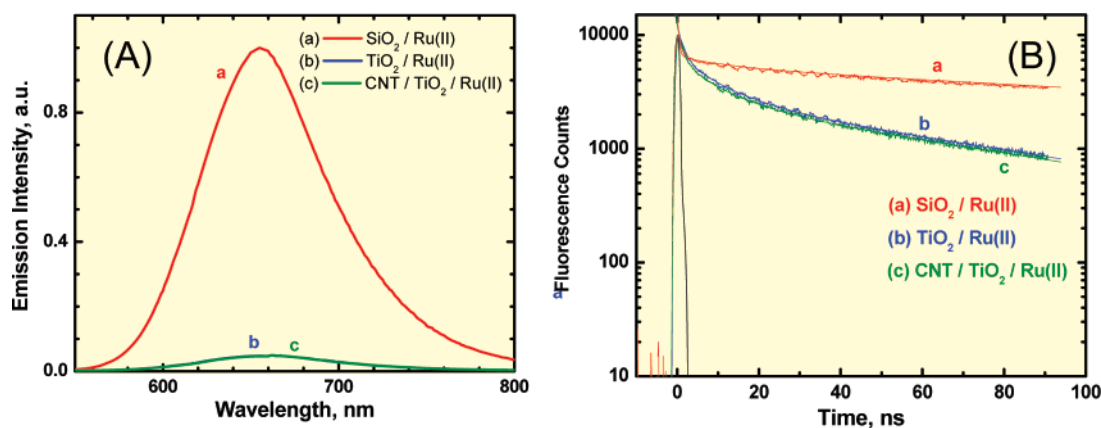


Figure 2. (A) Emission spectra (Ex. 470 nm, corrected for instrument response) and (B) emission decay at 655 nm of Ru(II)* on (a) SiO₂, (b) TiO₂, and (c) SWCNT/TiO₂ films.

demonstrate how the introduction of SWCNT scaffolding in the mesoscopic TiO₂ film influences the forward (reaction 3) and back (reaction 4) electron-transfer processes.

Emission Quenching of Excited Ru(II)* Complex. Figure 2A shows the emission spectra of Ru(II) bound to SiO₂, TiO₂, and SWCNT/TiO₂ films. Ru(II) bound to silica films exhibits an emission maximum at 655 nm as the excited dye undergoes deactivation via fluorescence. In contrast, the dye on the TiO₂ and SWCNT/TiO₂ surface exhibits decreased emission yield. More than 95% of the emission is quenched as the dye interacts with the TiO₂ surface and participates in the charge injection process (reaction 3). The similarity in quenching behavior between the TiO₂/Ru(II) and SWCNT/TiO₂/Ru(II) systems shows that the charge injection process is not significantly influenced by the presence of SWCNT in the film.

Figure 2B shows the emission decay of the Ru(II) complex at 655 nm following excitation with a 457-nm LED pulse (1

MHz repetition rate). The photon counts corresponding to the decay of Ru(II)* on oxide surfaces deviated from a single-exponential decay and thus were analyzed with a biexponential kinetic fit according to the expression: $y = a_1 \exp(-t/\tau_1) + a_2 \exp(-t/\tau_2)$. The Ru(II)* decays with a significantly faster rate when bound to the TiO₂ surface than on the SiO₂ surface.

As shown earlier, the deactivation of Ru(II)* on the surface of SiO₂ proceeds via reactions 1 and 2. The lifetime of Ru(II)* on SiO₂ is too long to be measured accurately on the time scale of this experiment but is estimated from nanosecond transient absorption measurements described later to be ~ 200 ns. On the other hand an additional deactivation pathway, the charge injection process (reaction 3), dominates on the TiO₂ surface. The Ru(II)* bound to TiO₂ deactivates with a faster rate, and the decay can be fitted to multiexponential kinetics. Earlier emission and microwave measurements have shown that the charge injection from the excited Ru(II)* complex into TiO₂

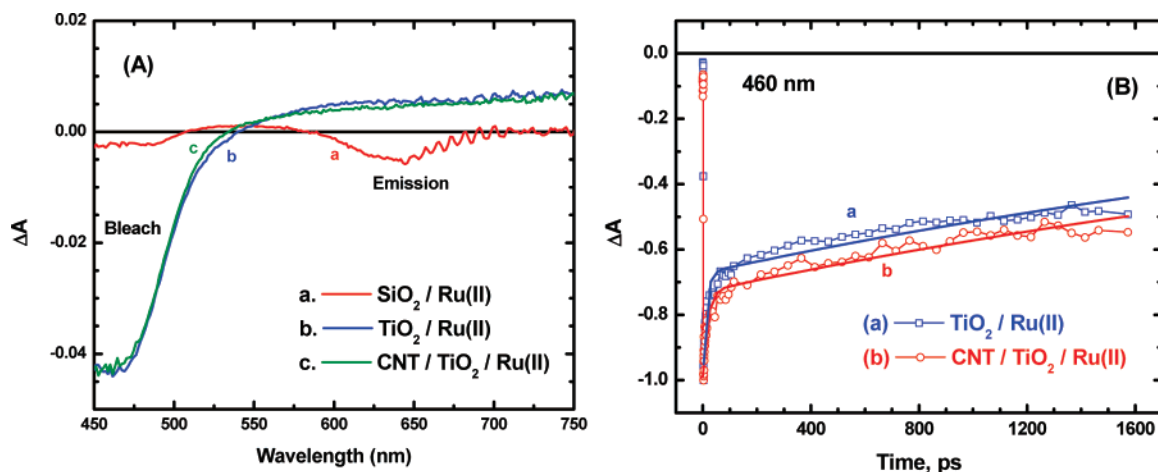


Figure 3. (A) Transient absorption spectra recorded 3 ps after 387-nm laser pulse excitation of Ru(II) complex anchored on (a) SiO₂, (b) TiO₂, and (c) SWCNT/TiO₂ films. (B) Comparison of normalized bleaching recovery traces monitored at 460 nm.

TABLE 1: Biexponential Decay Parameters for Emission Decay Lifetime

| | a_1 | τ_1 | a_2 | τ_2 | $\langle\tau\rangle$ |
|--------------------------------|-------|----------------|-------|---------------|----------------------|
| TiO ₂ /Ru(II) | 0.14 | 2.75 ± 0.06 ns | 0.86 | 27.9 ± 0.3 ns | 24.4 ± 0.2 ns |
| SWCNT/TiO ₂ /Ru(II) | 0.14 | 2.57 ± 0.05 ns | 0.86 | 28.1 ± 0.2 ns | 24.5 ± 0.2 ns |

TABLE 2: Biexponential Decay Parameters for Femtosecond Bleaching Recovery

| | a_1 | τ_1 | a_2 | τ_2 | $\langle\tau\rangle$ | R^2 |
|------------------------------|--------|-------------|--------|---------------|----------------------|-------|
| TiO ₂ /Ru(II) | -0.002 | 12 ± 1.4 ps | -0.998 | 3740 ± 220 ps | 3730 ± 220 ps | 0.980 |
| CNT/TiO ₂ /Ru(II) | -0.002 | 18 ± 3.3 ps | -0.998 | 4130 ± 295 ps | 4120 ± 290 ps | 0.967 |

occurs with a wide range of rate constants.⁴⁰ The surface heterogeneity and the nature of interaction between the sensitizer and semiconductor contribute to this multiexponential behavior.

The lifetimes of Ru(II)* decay on different films are compared in Table 1. The average decay lifetimes for the TiO₂/Ru(II) and SWCNT/TiO₂/Ru(II) films are 24.4 ± 0.2 ns and 24.5 ± 0.2 ns, respectively. Comparison of these fit parameters shows that the variation in the decay lifetimes is within the experimental error; hence, both of the lifetimes can be regarded as similar.

Femtosecond Pump-Probe Spectroscopy. Since the emission lifetime measurements in the above experiment could not resolve the ultrafast decay component, we further subjected the same samples to femtosecond pump-probe spectroscopy measurements. The transient absorption spectra recorded 3 ps after the 387 nm laser pulse excitation are shown in Figure 3A. The bleaching at 460 nm and absorption around 520 nm in the Ru(II)/SiO₂ film correspond to the excited Ru(II)*. In addition we also observe interference from the emission in the 580–680-nm region. On the other hand the Ru(II) deposited on TiO₂ and SWCNT/TiO₂ exhibits bleaching in the 460-nm region but no interference from the emission. On the TiO₂ surface the transient absorption is mainly dominated by both Ru(II)* and Ru(III) species. The broad absorption in the 700 nm region seen in the spectra of the TiO₂ and SWCNT/TiO₂ samples confirm the formation of electron-transfer products (trapped electrons and Ru(III) species) as the excited Ru(II)* undergoes electron transfer with TiO₂ (Reaction 3).

Figure 3B shows the bleaching recovery recorded at 460 nm. This initial fast recovery represents the ultrafast component of the charge injection process. Once again, we see a multiexponential kinetic behavior, and the traces were analyzed using the same biexponential kinetic fit. The lifetimes are summarized in Table 2. The short component of ~15 ps and the longer component of a lifetime of ~4000 ps are similar in both the TiO₂ and SWCNT/TiO₂ samples. These results support the argument made in the previous section that the excited-state

deactivation of the Ru(II) complex is mainly dominated by the charge-transfer interaction with TiO₂, while the presence of the SWCNT does not significantly affect the charge injection rate. It is apparent that the rate of charge injection from Ru(II)* to TiO₂ is much faster than that from TiO₂ to SWCNT, explaining why no noticeable change in the lifetime of the excited-state is observed.

Back Electron Transfer. Although SWCNT does not influence the primary charge injection process in the Ru(II)*-TiO₂ system, one expects its participation in facilitating charge separation and in promoting electron transport to the electrode surface. Its ability to accept electrons from UV-irradiated TiO₂ has been demonstrated in our earlier investigation.^{29,30} If, indeed, SWCNT should collect photoinjected electrons from the TiO₂/

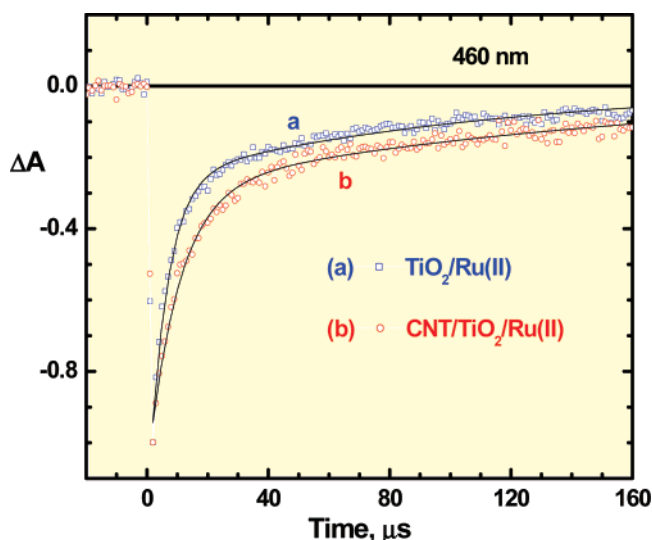


Figure 4. Normalized absorption-time profile at 460 nm showing the bleaching recovery of OTE/TiO₂/Ru(II) and OTE/SWCNT/TiO₂/Ru(II) electrodes (degassed) following 355-nm laser pulse excitation.

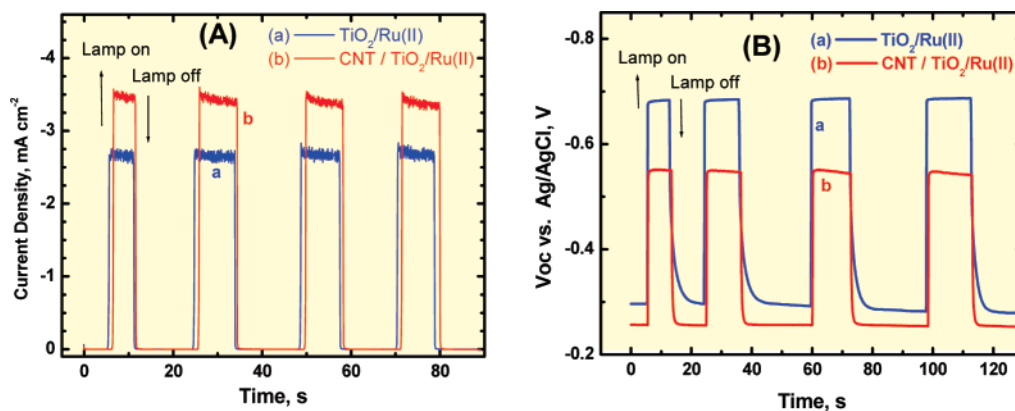


Figure 5. (A) Photocurrent and (B) photovoltage response of (a) OTE/TiO₂/Ru(II) and (b) OTE/SWCNT/TiO₂/Ru(II) electrodes. Light intensity was 100 mW/cm² ($\lambda > 400$ nm). Electrolyte was 0.5 M LiI and 0.05 M I₂ in acetonitrile.

SCHEME 2: Energy Diagram Illustrating the Charge Injection from Excited Sensitizer (S*) into TiO₂ and Transport of Photoinjected Electrons to the Electrode Surface without (a) and with (b) SWCNT Network (The Fermi Level of TiO₂ (E_f') Shifts to More Positive Potentials (E_f'') as It Equilibrates with SWCNT)

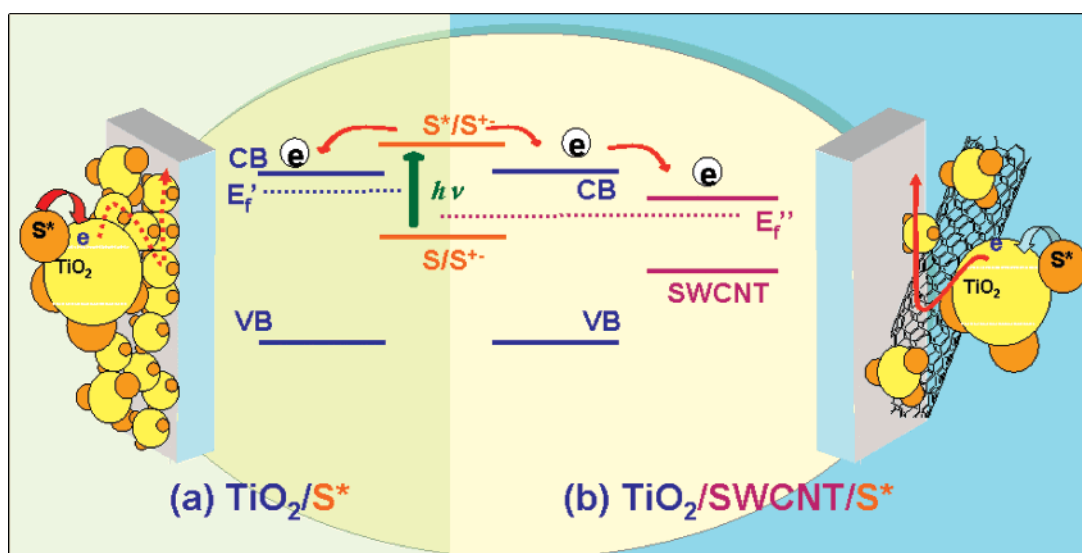


TABLE 3: Biexponential Decay Parameters for Nanosecond Bleaching Recovery

| | a_1 | τ_1 | a_2 | τ_2 | $\langle \tau \rangle$ | R^2 |
|------------------------------|-------|----------------------------|-------|-------------------------|-------------------------|-------|
| TiO ₂ /Ru(II) | -0.17 | $6.0 \pm 0.1 \mu\text{s}$ | -0.83 | $110 \pm 4 \mu\text{s}$ | $93 \pm 4 \mu\text{s}$ | 0.983 |
| CNT/TiO ₂ /Ru(II) | -0.15 | $10.2 \pm 0.4 \mu\text{s}$ | -0.85 | $159 \pm 8 \mu\text{s}$ | $137 \pm 7 \mu\text{s}$ | 0.987 |

Ru(II)* system, we should be able to see an improved charge separation in SWCNT/TiO₂/Ru(II) films.

We employed nanosecond laser flash photolysis to probe the charge separation process by monitoring the long-term stability of the photogenerated electron-transfer products. One of the major factors that dictate the performance of DSSCs is the back electron transfer.^{44,49–51} As shown earlier, the back electron transfer (reaction 4) between Ru(III) and TiO₂(e) occurs over a time scale of microseconds to milliseconds.⁵⁰ This process is readily followed by monitoring the recovery of the bleaching at 460 nm since the contribution of the excited species at this long time scale is negligible. Figure 4 shows the time-resolved transient spectra recorded in a nanosecond laser flash photolysis experiment using a 355-nm laser pulse excitation. The Ru(II) complex loaded films were inserted into a spectroscopic cell that was degassed by applying vacuum. Evacuation of the sample cell ensured that there was no scavenging of electrons by oxygen. The spectral characteristics of the transient absorption were similar in both films and the recovery continued for hundreds of microseconds. Since the excited-state is the only

transient formed in SiO₂ films due to the large band gap of SiO₂, no long-lived species could be seen in the microsecond time scale for the SiO₂/Ru(II) films.

The transient recovery of Ru(II) in evacuated TiO₂ and SWCNT/TiO₂ films are compared in Figure 4. The recovery recorded during first 160 μs was analyzed using biexponential kinetics, and the lifetime values are summarized in Table 3. Both the short component and the long component of the recovery were slower when the film contained a SWCNT network. The average lifetime of the Ru(II) recovery corresponding to reaction 4 was 93 μs for TiO₂ films and 137 μs for SWCNT/TiO₂ films. These results suggest that the photoinjected electrons in TiO₂ survive roughly 50% longer when embedded within the SWCNT network. The equilibration of electrons between SWCNT and TiO₂ results in the transfer of a fraction of electrons into SWCNT, thus stabilizing the photogenerated electrons and reducing the rate of exciton recombination.

Photoelectrochemical Activity of Ru(II) Complex-Modified TiO₂ and TiO₂/SWCNT Films. To probe the beneficial aspect of a SWCNT network in DSSCs, we constructed

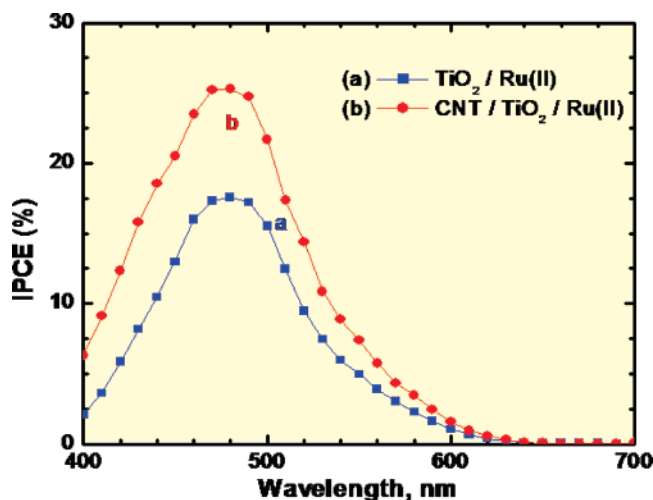


Figure 6. Photocurrent action spectra of (a) OTE/TiO₂/Ru(II) and (b) OTE/SWCNT/TiO₂/Ru(II) electrodes. IPCE (%) = $(1240i_{sc})/(\lambda I_{inc}) \times 100$ where i_{sc} is short circuit current and I_{inc} is the power of the incident light. Electrolytes were 0.5 M LiI and 0.05 M I₂ in acetonitrile.

photoelectrochemical cells using the Ru(II)-modified TiO₂ particulate films described previously as photoanodes. The magnitude of the photocurrent response represents the charge collection efficiency at the electrode surface. Figure 5A shows the short-circuit photocurrent generation of the OTE/TiO₂/Ru(II) and OTE/SWCNT/TiO₂/Ru(II) electrodes. Both electrodes were prompt in generating photocurrent with a reproducible response to ON–OFF cycles. It is interesting to note that the films containing a SWCNT network exhibited a roughly 30% higher photocurrent. (Note that this increase is greater than the small (2.3%) difference in absorbance between TiO₂/Ru(II) and SWCNT/TiO₂/Ru(II) films). On the other hand, the photovoltage (Figure 5B) recorded during ON–OFF cycles shows a decreased open-circuit voltage when SWCNT was present in the film.

The two opposing trends seen in the short-circuit current and open-circuit voltage (Figure 5) can be explained on the basis of the electron capture properties of SWCNT. As the photo-injected electrons are transferred to TiO₂ from excited Ru(II)*, they undergo charge equilibration with SWCNT. As demonstrated in an earlier study, this charge equilibration is associated with the shifting of the apparent Fermi level to more positive potentials.^{29,31} A positive shift of tens to hundreds of millivolts in the apparent Fermi level has been noted from the redox equilibration experiments. This shift causes the open-circuit voltage of the photoelectrochemical cell, which is dependent on the difference in Fermi levels between the photoanode and the redox couple, to be lower than that obtained in the absence of SWCNT. The electrons transferred into the SWCNT network are quickly transported to the collecting electrode surface, minimizing the possibility of charge recombination at grain boundaries. The incorporation of a SWCNT network in the TiO₂ film thus helps to transport electrons through its conductive scaffold and to generate higher photocurrent, at the expense of the open-circuit potential (Scheme 2).

We further evaluated the electrode performance by recording the incident photon to charge carrier conversion efficiency (IPCE) at different incident wavelengths of light. The photocurrent action spectra of the two electrodes under unbiased conditions are shown in Figure 6. Both these electrodes exhibit an IPCE maximum corresponding to the absorption maximum of the Ru(II) complex. The IPCE response at all wavelengths is enhanced by a factor of ~ 1.4 as a result of introducing a

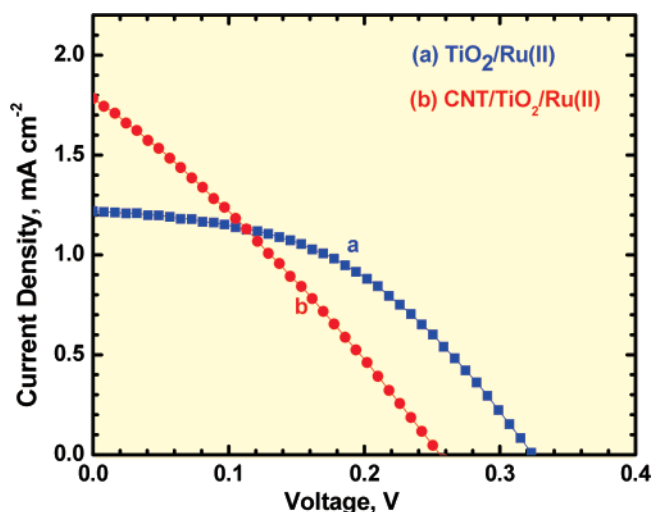


Figure 7. Power characteristics of a photoelectrochemical cell employing (a) OTE/TiO₂/Ru(II) and (b) OTE/SWCNT/TiO₂/Ru(II) electrodes. Electrolyte was 0.5 M LiI and 0.05 M I₂ in acetonitrile.

SWCNT scaffold in the mesoscopic TiO₂ film. Factors controlling the IPCE in DSSC solar cells have been discussed in detail by several research groups.^{3–5,52,53} Suppressing the back electron transfer and improving the electron transport within the nanostructured TiO₂ film are regarded as the two most important factors controlling the overall IPCE of the cell. Enhancement in the photoconversion efficiency in the present experiments suggests that charge collection and transport in these films are improved by the SWCNT network.

We also evaluated the power characteristics by varying the load resistance (Figure 7). A 45% increase in short circuit current seen with the SWCNT nanostructure is consistent with the IPCE and photocurrent measurements described earlier. However, the open-circuit voltage is decreased by about 60 mV as a result of charge of equilibration between TiO₂ and SWCNT.⁵⁴ A shift in open-circuit potential was also noted in UV-irradiated SWCNT–TiO₂ films.⁵⁵ Since the conduction band of SWCNT (~ 0 V vs NHE) is expected to be more positive than that of TiO₂ (-0.5 V vs NHE), we expect charge equilibration between the two systems causing the shift of apparent Fermi level to more positive potentials. Spectroscopic and photoelectrochemical measurements have also confirmed the ability of SWCNT to accept electrons and undergo charge equilibration.^{21,29,30,32} The power conversion efficiency for the DSSC's employing OTE/TiO₂/Ru(II) and OTE/SWCNT/TiO₂/Ru(II) electrodes were 0.18 and 0.13%, respectively. The similarity between these two values suggests that any improvement in photocurrent is nullified by the decrease in photovoltage. As a result of these opposing factors we see a small decrease in the fill factor and net power conversion efficiency.

Although the overall performance of SWCNT-based scaffolding is rather limited in DSSC, the results described in this study highlight the importance of 1-D nanostructures in improving the charge transport. Ideally, one needs to pick a 1-D system that matches the conduction band of TiO₂. In fact recent studies carried out with TiO₂^{12,56–58} and ZnO nanotubes^{13–15} suggest the possibility of improving the charge transport in DSSC. More work is needed to implement 1-D structures into photochemical solar cells.

Conclusions

SWCNT support networks can be incorporated into mesoscopic TiO₂ films to improve the charge transport in DSSC.

While no net increase in power conversion efficiency is seen, an increase in photon-to-current efficiency (IPCE) represents the beneficial role of the SWCNT as a conducting scaffold to facilitate charge separation and charge transport in nanostructured semiconductor films. Such nanowire/nanoparticle architecture is likely to play an important role in improving the efficiency of nanostructure-based solar energy conversion devices such as DSSCs and quantum dot solar cells and in water photoelectrolysis.

Acknowledgment. The research described herein was supported by the Office of Basic Energy Science of the Department of the Energy. P.B. gratefully acknowledges the support of the Vincent P. Slatt Undergraduate Research Fellowship provided by the Notre Dame Energy Center. We also would like to thank Toyota Central R&D Labs., Aichi, Japan, for the generous research grant enabling the stay of T.K. at Notre Dame. This is contribution NDRL-4754 from the Notre Dame Radiation Laboratory.

References and Notes

- (1) Kamat, P. V. *J. Phys. Chem. C* **2007**, *111*, 2834.
- (2) Graetzel, M. *Nature* **2001**, *414*, 338.
- (3) Bisquert, J.; Cahen, D.; Hodes, G.; Rühle, S.; Zaban, A. *J. Phys. Chem. B* **2004**, *108*, 8106.
- (4) Meyer, G. J. *Inorg. Chem.* **2005**, *44*, 6852.
- (5) Gratzel, M. *Inorg. Chem.* **2005**, *44*, 6841.
- (6) Gratzel, M. *J. Photochem. Photobiol. A* **2004**, *164*, 3.
- (7) Heimer, T. A.; Heilweil, E. J.; Bignozzi, C. A.; Meyer, G. J. *J. Phys. Chem. A* **2000**, *104*, 4256.
- (8) Kamat, P. V.; Haria, M.; Hotchandani, S. *J. Phys. Chem. B* **2004**, *108*, 5166.
- (9) Sirbully, D. J.; Law, M.; Yan, H.; Yang, P. *J. Phys. Chem. B* **2005**, *109*, 15190.
- (10) Law, M.; Greene, L. E.; Johnson, J. C.; Saykally, R.; Yang, P. *Nature Mater.* **2005**, *4*, 455.
- (11) Klimov, V. I. *J. Phys. Chem. B* **2006**, *110*, 16827.
- (12) Mor, G. K.; Shankar, K.; Paulose, M.; Varghese, O. K.; Grimes, C. A. *Nano Lett.* **2006**, *6*, 215.
- (13) Galoppini, E.; Rochford, J.; Chen, H.; Saraf, G.; Lu, Y.; Hagfeldt, A.; Boschloo, G. *J. Phys. Chem. B* **2006**, 16159.
- (14) Martinson, A. B. F.; Elam, J. W.; Hupp, J. T.; Pellin, M. J. *Nano Lett.* **2007**, *7*, 2183.
- (15) Martinson, A. B. F.; Elam, J. W.; Hupp, J. T.; Pellin, M. J. *Nano Lett.* **2007**, *7*, 2183.
- (16) Romanov, S. G.; Sotomayor Torres, C. M.; Yates, H. M.; Pemble, M. E.; Butko, V.; Tretijakov, V. *J. Appl. Phys.* **1997**, *82*, 380.
- (17) Leschkes, K. S.; Divakar, R.; Basu, J.; Enache-Pommer, E.; Boercker, J. E.; Carter, C. B.; Kortshagen, U. R.; Norris, D. J.; Aydil, E. S. *Nano Lett.* **2007**, *7*, 1793.
- (18) Hoppe, H.; Sariciftci, N. S. *J. Mater. Res.* **2004**, *19*, 1924.
- (19) Girishkumar, G.; Hall, T. D.; Vinodgopal, K.; Kamat, P. V. *J. Phys. Chem. B* **2006**, *110*, 107.
- (20) Kongkanand, A.; Vinodgopal, K.; Kuwabata, S.; Kamat, P. V. *J. Phys. Chem. B* **2006**, *110*, 16185.
- (21) Robel, I.; Bunker, B.; Kamat, P. V. *Adv. Mater.* **2005**, *17*, 2458.
- (22) Olek, M.; Busgen, T.; Hilgendorff, M.; Giersig, M. *J. Phys. Chem. B* **2006**, *110*, 12901.
- (23) Ravindran, S.; Chaudhary, S.; Colburn, B.; Ozkan, M.; Ozkan, C. S. *Nano Lett.* **2003**, *3*, 447.
- (24) Haremza, J. M.; Hahn, M. A.; Krauss, T. D. *Nano Lett.* **2002**, *2*, 1253.
- (25) Banerjee, S.; Wong, S. S. *Chem. Commun.* **2004**, 1866.
- (26) Shen, Q.; Katayama, K.; Sawada, T.; Yamaguchi, M.; Toyoda, T. *Jpn. J. Appl. Phys.* **2006**, *45*, 5569–5574.
- (27) Guldi, D. M.; Rahman, G. M. A.; Sgobba, V.; Kotov, N. A.; Bonifazi, D.; Prato, M. *J. Am. Chem. Soc.* **2006**, *128*, 2315.
- (28) Grzelczak, M.; Correa-Duarte, M. A.; Salgueiriño-Maceira, V.; Giersig, M.; Diaz, R.; Liz-Marzán, L. M. *Adv. Mater.* **2006**, *18*, 415.
- (29) Kongkanand, A.; Kamat, P. V. *ACS Nano* **2007**, *1*, 13.
- (30) Kongkanand, A.; Kamat, P. V. *J. Phys. Chem. C* **2007**, *111*, 9012.
- (31) Kongkanand, A.; Domínguez, R. M.; Kamat, P. V. *Nano Lett.* **2007**, *7*, 676.
- (32) Vietmeyer, F.; Seger, B.; Kamat, P. V. *Adv. Mater.* **2007**, *19*, 2935.
- (33) Hasobe, T.; Imahori, H.; Kamat, P. V.; Fukuzumi, S. *J. Am. Chem. Soc.* **2005**, *127*, 1216.
- (34) Hasobe, T.; Kamat, P. V.; Troiani, V.; Solladie, N.; Ahn, T. K.; Kim, S. K.; Kim, D.; Kongkanand, A.; Kuwabata, S.; Fukuzumi, S. *J. Phys. Chem. B* **2005**, *109*, 19.
- (35) Hasobe, T.; Fukuzumi, S.; Kamat, P. V. *J. Am. Chem. Soc.* **2005**, *127*, 11884.
- (36) Hasobe, T.; Fukuzumi, S.; Kamat, P. V. *J. Phys. Chem. B* **2006**, *110*, 25477.
- (37) Kamat, P. V.; Thomas, K. G.; Barazzouk, S.; Girishkumar, G.; Vinodgopal, K.; Meisel, D. *J. Am. Chem. Soc.* **2004**, *126*, 10757.
- (38) Kamat, P. V. *J. Phys. Chem.* **1989**, *93*, 859.
- (39) Kamat, P. V.; Gopidas, K. R.; Weir, D. *Chem. Phys. Lett.* **1988**, *149*, 491.
- (40) Fessenden, R. W.; Kamat, P. V. *J. Phys. Chem.* **1995**, *99*, 12902.
- (41) Randy, J.; Ellingson, R. J.; Asbury, J. B.; Ferrere, S.; Ghosh, H. N.; Sprague, J. R.; Lian, T.; Nozik, A. J. *J. Phys. Chem. B* **1998**, *102*, 6455.
- (42) Hilgendorff, M.; Sundström, V. *J. Phys. Chem. B* **1998**, *102*, 10505.
- (43) Hannappel, T.; Burfeindet, B.; Storck, W.; Willig, F. *J. Phys. Chem. B* **1997**, *101*, 6799.
- (44) Yan, S. G.; Hupp, J. T. *J. Phys. Chem.* **1996**, *100*, 6867.
- (45) Martini, I.; Hodak, J.; Hartland, G.; Kamat, P. V. *J. Chem. Phys.* **1997**, *107*, 8064.
- (46) Tachibana, Y.; Haque, S. A.; Mercer, I. P.; Durrant, J. R.; Klug, D. R. *J. Phys. Chem. B* **2000**, *104*, 1198.
- (47) Krüger, J.; Plass, R.; Grätzel, M.; Cameron, P. J.; Peter, L. M. *J. Phys. Chem. B* **2003**, *107*, 7536.
- (48) Kopidakis, N.; Benkstein, K. D.; Lagemaat, J. v. d.; Frank, A. J. *J. Phys. Chem. B* **2003**, *107*, 11307.
- (49) Haque, S. A.; Tachibana, Y.; Klug, D. R.; Durrant, J. R. *J. Phys. Chem. B* **1998**, *102*, 1745.
- (50) Nasr, C.; Hotchandani, S.; Kamat, P. V. *J. Phys. Chem. B* **1998**, *102*, 4944.
- (51) Bergeron, B. V.; Marton, A.; Oskam, G.; Meyer, G. J. *J. Phys. Chem. B* **2005**, *109*, 937.
- (52) Kamat, P. V.; Bedja, I.; Hotchandani, S.; Patterson, L. K. *J. Phys. Chem.* **1996**, *100*, 4900.
- (53) Cahen, D.; Graetzel, M.; Guillemoles, J. F.; Hodes, G. *Dye Sensitized Solar Cells: Principles of Operation*. In *Electrochemistry of Nanomaterials*; Hodes, G., Ed.; Wiley-VCH Verlag GmbH: Weinheim, 2001; p 201.
- (54) Jung, K. H.; Hong, J. S.; Vittal, R.; Kim, K. J. *Chem. Lett.* **2002**, 864.
- (55) Kongkanand, A.; Kuwabata, S.; Girishkumar, G.; Kamat, P. *Langmuir* **2006**, *21*, 2392.
- (56) Mor, G. K.; Varghese, O. K.; Paulose, M.; Shankar, K.; Grimes, C. A. *Sol. Energy Mater. Solar Cells* **2006**, *90*, 2011.
- (57) Uchida, S.; Chiba, R.; Tomiha, M.; Masaki, N.; Shirai, M. *Electrochemistry* **2002**, *70*, 418.
- (58) Tan, B.; Wu, Y. *J. Phys. Chem. B* **2006**, *110*, 15932.